A Patient-Specific Modeling Pipeline for Non-Ischemic Cardiomyopathy

Riccardo Mariani[1], Chiara Celotto[1], Diego Penela[2], Jose F. Rodriguez Matas[1]

[1] LaBS, Department of Chemistry, Materials and Chemical Engineering "Giulio Natta", Politecnico di Milano, Milan, Italy
[2] IRCCS Humanitas Research Hospital, Milan, Italy

Abstract

Non-ischemic cardiomyopathy (NICM) may produce an electrically heterogeneous myocardial scar containing slow-conducting channels (SCCs). We developed a patient-specific left ventricular (LV) model of a subject with NICM secondary to acute myocarditis and compared three representations of the fibrotic substrate.

Nine LGE-derived surface meshes provided the geometry and normalized damage map. The scalar field was interpolated onto a 2.4-million-element hexahedral mesh with 0.4 mm target edge length. Rule-based fibers and a Laplacian transmural coordinate defined ventricular cell types. Tissue conductivities were calibrated to longitudinal and transverse conduction velocities of 65 and 50 cm/s. Fibrotic remodeling was represented by conductivity reduction, explicit MacCannell fibroblasts coupled to myocytes, or their combination.

The healthy model activated in approximately 170 ms. The pathological models preserved total activation time but produced distinct local propagation patterns. Conductivity reduction fragmented the wavefront, fibroblast coupling produced a more diffuse wavefront, and their combination caused the largest local conduction retardation. The complete model reproduced the spatial location of the clinically identified SCC while maintaining conduction through the channel.

1. Introduction

Non-ischemic cardiomyopathy (NICM) encompasses a heterogeneous group of myocardial diseases ranging from genetic to inflammatory etiologies, unrelated to coronary artery disease and it is associated with ventricular tachycardia (VT) and sudden cardiac death. NICM may alter electrophysiological conduction pathways through myocardial scar formation. The scar is characterized by a dense fibrotic core surrounded by a border zone (BZ) containing damaged myocytes with altered electrical properties, resulting in an electrically heterogeneous substrate. Surviving myocytes embedded within the scar may form slow-conducting channels (SCCs), which allow propagation along non-physiological pathways and can facilitate reentry.

Catheter ablation is used to control VT by targeting SCCs supporting reentrant circuits. However, clinical imaging may not accurately localize patient-specific arrhythmogenic regions, complicating SCC identification [1]. Patient-specific computational models can provide a complementary framework for characterizing the electrophysiological substrate and evaluating its response to stimulation.

Fibrotic remodeling can be represented by reduced tissue conductivity, by electrotonic coupling between myocytes and fibroblasts, or by both mechanisms. Comparing these representations within the same anatomy allows their individual effects on activation to be distinguished.

This work presents a patient-specific computational modeling pipeline for a subject affected by NICM secondary to acute myocarditis. LGE-MRI data are integrated into a high-resolution LV model including patient-specific geometry, fiber orientation, and transmural heterogeneity. Three representations of the fibrotic substrate are compared and the resulting activation patterns are evaluated against the clinical substrate and SCC.

2. Methods

Figure 1 summarizes the main steps of the patient-specific modeling pipeline, from LGE-MRI-derived geometry and tissue damage mapping to fiber assignment, transmural heterogeneity, fibroblast distribution, and ventricular stimulation.

2.1. Clinical data

The model is based on a patient who developed multiple VT episodes following acute myocarditis, resulting in scar formation in the posterolateral wall of the LV [2]. LGE-MRI provided nine VTK surface meshes sampled at different depths through the LV wall. Each mesh point was associated with a scalar value in $[0, 1]$ representing local

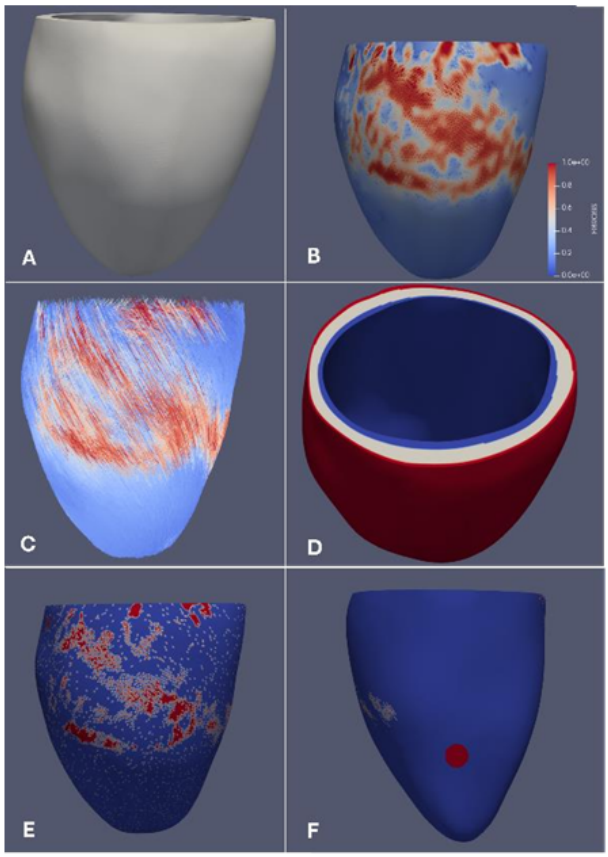

Figure 1. Main steps of the patient-specific modeling pipeline: (A) LV geometry; (B) interpolated damage map; (C) fiber orientation; (D) transmural heterogeneity (epicardium red, mid-myocardium white, endocardium blue); (E) fibroblast distribution (red) in healthy myocardium (blue); (F) apical-septal stimulation region.

tissue damage, with higher values corresponding to greater damage.

2.2. Geometry, mesh and scalar mapping

The outermost and innermost surfaces were used to define the epicardial and endocardial boundaries, respectively. A planar basal cut was performed to regularize the upper boundary while preserving the fibrotic region of interest. The LV volume between the two surfaces was generated in ANSA v23.1.1 (BETA CAE Systems).

The patient-specific geometry was subsequently meshed in ANSA by partitioning the LV into eight slices starting from a truncated cone at the apex, to reduce curvature variation and improve mesh regularity. Linear hexahedral elements with a 0.4 mm target edge length yielded 2 416 860 elements and 2 543 352 nodes, using a resolution previously proved accurate enough by our group [3].

The VTK scalar values were mapped to the nearest volumetric nodes within a 0.5 mm cube using Matlab R2025 (The MathWorks, Inc.). The mapped nodes were imposed as Dirichlet boundary conditions for a steady-state heat-diffusion problem, producing a smooth scalar field throughout the LV while preserving the input distribution.

2.3. Fiber orientation and transmural heterogeneity

Fiber orientation was computed following Wong and Kuhl [4]. A local cardiac coordinate system was defined on the epicardial and endocardial surfaces, and helix angles of -60° and $+60^\circ$ were prescribed, respectively. The three components of the fiber vector were then interpolated through the LV wall by solving independent Poisson problems.

To define transmural heterogeneity, a transmural coordinate ρ was computed by steady-state heat diffusion with $\rho = 0$ at the endocardium and $\rho = 1$ at the epicardium. This coordinate defines the relative transmural position independently of local variations in wall thickness. Nodes were classified as endocardial, mid-myocardial, or epicardial according to ρ. The mid-myocardial region occupied 60% of wall thickness, accounting for the higher prevalence of M-cells [5].

2.4. Conduction velocity calibration

Longitudinal (σ_l) and transverse (σ_t) conductivities were calibrated with monodomain simulations in ELVIRA [6] on a 0.4 mm-meshed rectangular tissue prism. Target conduction velocities were 65 cm/s along and 50 cm/s across the fibers [7], resulting in $\sigma_l = 1.80 \cdot 10^{-3}$ and $\sigma_t = 1.26 \cdot 10^{-3}$.

2.5. Pathological substrate modeling

For each hexahedral element, the mean damage $\overline{s}$ of its eight nodes was computed. Elements with $\overline{s} < 0.7$ were considered healthy. For $\overline{s} \geq 0.7$, the number of pathological nodes was determined by

$$N = \frac{8}{1 + e^{-\kappa(\overline{s} - F)}}, \tag{1}$$

with $\kappa = 20$ and $F = 0.92$. The resulting value was rounded upward and assigned to the nodes with the highest scalar values.

Three configurations were defined from the same damage field. In the *conductivity-based* model, σ_l and σ_t were reduced according to damage, from the healthy calibrated values to zero. In the *cellular-based* model, the MacCannell fibroblast model [8] was assigned to flagged nodes

while conductivity remained at healthy values; an additional 3% of nodes was assigned fibroblasts to represent diffuse physiological fibrosis [9]. The *full* model combined both mechanisms, with conductivity reduced to no less than one quarter of the healthy value.

2.6. Simulation setup

Ventricular myocytes were represented by the Ten Tusscher-Panfilov model [10], with epicardial, mid-myocardial, and endocardial cell types. Fibroblasts used the MacCannell model. The LV was stimulated at the apical-septal region with 380 μA/cm^2 for 2 ms, reproducing the position of a catheter in the septum of right ventricle during clinical pacing. All models were preconditioned for six beats at an 800 ms basic cycle length before the activation sequence analyzed in this study.

3. Results

3.1. Healthy baseline

The healthy LV activated from the apical-septal stimulation site toward the base with a stable elliptical pattern, consistent with the prescribed fiber orientation. The TAT was approximately 170 ms. Clinical consultation indicated an LV TAT of 115–130 ms for apical-septal pacing. The longer simulated value is attributable to the absence of the His-Purkinje system and the single stimulation site, so propagation relies entirely on myocardial conduction.

3.2. Comparison of the three pathological substrates

The three pathological configurations were stimulated using the same protocol. Figure 2 compares the activation wavefront at $t = 140$ ms, while the impulse is propagating through the scarred region.

The conductivity-based model produced a fragmented wavefront and zig-zag propagation around non-conducting regions associated with the highest damage levels. In the cellular-based model, the wavefront became more diffuse. This behavior is consistent with the electrotonic current sink introduced by fibroblasts, which diverts part of the depolarizing current from the myocytes and reduces local conduction velocity without producing the same fragmentation.

The full model combined the two effects. The wavefront propagated through narrow pathways defined by the structural barriers, while fibroblast electrotonic loading further delayed propagation within these pathways, producing the largest local conduction retardation.

Despite these local differences, TAT did not significantly increase relative to the healthy model. Thus, global activation remained preserved while propagation within the scar was locally altered.

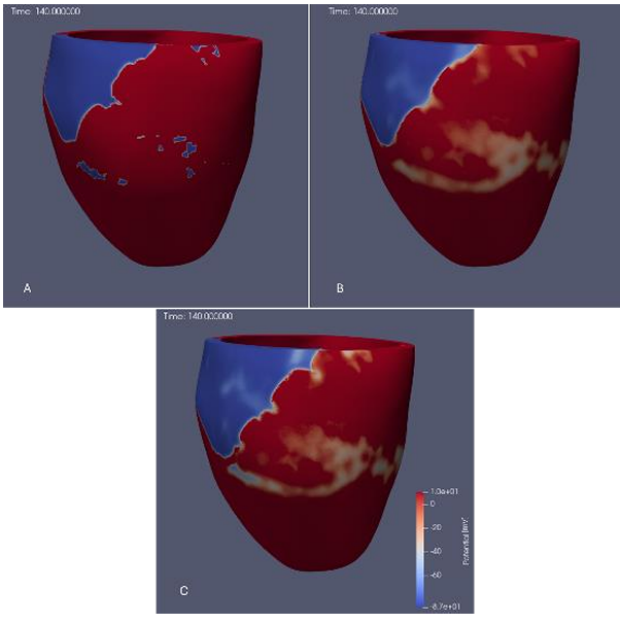

Figure 2. Transmembrane potential at $t = 140$ ms in the three pathological substrates: (A) conductivity-based remodeling, (B) cellular-based remodeling, (C) full pathological substrate model.

3.3. Comparison with the clinical substrate

The full model reproduced a slow-conducting channel within the posterior-lateral scar, spatially corresponding to the clinically identified isthmus (Figure 3). Overlay of the clinical isthmus path on the simulated activation map showed a high degree of spatial correspondence. The wavefront remained conductive within the channel rather than being blocked, providing the basis for subsequent VT induction simulations.

4. Discussion

The three substrate representations preserved global activation time but produced distinct local propagation patterns, showing that TAT alone is insufficient to discriminate between NICM substrate models. Conductivity reduction introduced non-conducting regions and wavefront fragmentation, whereas fibroblast–myocyte coupling reduced local conduction through electrotonic loading. Their combination reproduced narrow conductive pathways and local conduction retardation, with spatial correspondence to the clinical SCC.

These results indicate that structural and cellular remodeling alter the propagating wavefront in distinct ways:

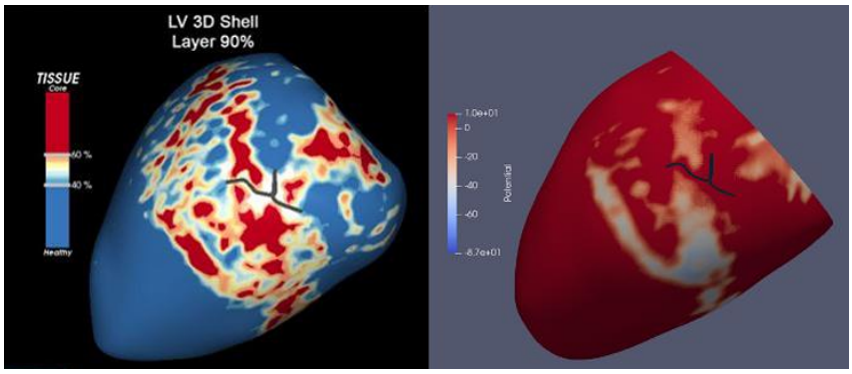

Figure 3. Clinical electroanatomical map of the 90% shell with the clinically identified isthmus path (black line), left, and simulated transmembrane potential in the complete pathological substrate, right.

the conductivity reduction fragments it along a zig-zag path, whereas fibroblast coupling makes it more diffuse without producing fragmentation. The full representation combines both effects within the same patient-specific anatomy, preserves a total activation time consistent with the healthy baseline, and reproduces the slow-conducting channel clinically identified within the posterolateral scar.

This single-patient study is primarily qualitative. Quantitative assessment of conduction velocity and activation delay within the clinical isthmus would strengthen validation. The model lacks the His-Purkinje system and pathological flags and thresholds are derived from LGE rather than histology. Future work will apply programmed stimulation for VT induction to the complete substrate.

5. Conclusions

A patient-specific LV electrophysiological model was developed for NICM from LGE-MRI data and used to compare conductivity-based, cellular-based, and combined fibrotic remodeling. All configurations preserved global activation time but produced distinct local propagation patterns. The full model combined structural barriers with fibroblast-induced conduction retardation and reproduced the clinically identified SCC while maintaining conduction. The model provides a platform for subsequent VT induction simulations.

Acknowledgments

Computations were performed at the computing facilities of DCMC at Politecnico di Milano.

References

[1] Desjardins B, Yokokawa M, Good E, Crawford T, Latchamsetty R, Jongnarangsin K, Ghanbari H, Oral H, Pelosi F Jr, Chugh A, Morady F, Bogun F. Characteristics of intramural scar in patients with nonischemic cardiomyopathy and relation to intramural ventricular arrhythmias. *Circ Arrhythm Electrophysiol* 2013;6:891–897.

[2] Falasconi G, et al. Cardiac magnetic resonance-aided epicardial ventricular tachycardia ablation in post-myocarditis patient. *J Interv Card Electrophysiol* 2023;67:249–251.

[3] Tobar AM, Ferrero JM, Migliavacca F, Rodríguez Matas JF. Vulnerability in regionally ischemic human heart. Effect of the extracellular potassium concentration. *J Comput Sci* 2018;24:160–168.

[4] Wong J, Kuhl E. Generating fibre orientation maps in human heart models using Poisson interpolation. *Comput Methods Biomech Biomed Engin* 2014;17:1217–1226.

[5] Glukhov AV, et al. Transmural dispersion of repolarization in failing and nonfailing human ventricle. *Circ Res* 2010;106:981–991.

[6] Heidenreich EA, Ferrero JM, Doblaré M, Rodríguez JF. Adaptive macro finite elements for the numerical solution of monodomain equations in cardiac electrophysiology. *Ann Biomed Eng* 2010;38:2331–2345.

[7] Taggart P, et al. Inhomogeneous transmural conduction during early ischaemia in patients with coronary artery disease. *J Mol Cell Cardiol* 2000;32:621–630.

[8] MacCannell KA, Bazzazi H, Chilton L, Shibukawa Y, Clark RB, Giles WR. A mathematical model of electrotonic interactions between ventricular myocytes and fibroblasts. *Biophys J* 2007;92:4121–4132.

[9] Fan D, Takawale A, Lee J, Kassiri Z. Cardiac fibroblasts, fibrosis and extracellular matrix remodeling in heart disease. *Fibrogenesis Tissue Repair* 2012;5:15.

[10] Ten Tusscher KHWJ, Panfilov AV. Alternans and spiral breakup in a human ventricular tissue model. *Am J Physiol Heart Circ Physiol* 2006;291:H1088–H1100.

Address for correspondence:

Jose F Rodriguez Matas
Politecnico di Milano, Piazza Leonardo da Vinci 32, 20133 Milan, Italy
josefelix.rodriguezmatas@polimi.it